Tribology Letters (2021) 69:72
https://doi.org/10.1007/s11249-021-01446-6

ORIGINAL PAPER

An Assessment of the Effect of Relative Humidity on the Decomposition of the ZDDP Antiwear Additive

Abdel Dorgham[1] · Abdullah Azam[1] · Pourya Parsaeian[1] · Chun Wang[1] · Ardian Morina[1] · Anne Neville[1]

Received: 12 January 2021 / Accepted: 18 April 2021 / Published online: 8 May 2021

Abstract

The effect of relative humidity on the decomposition reaction of zinc dialkyldithiophosphate (ZDDP) additive under boundary lubrication regime has been investigated using Raman spectroscopy and atomic force microscopy (AFM). The ZDDP tribofilms were formed using the pin-on-disc tribometer at 30 and 90% relative humidity, which was controlled using a custom-made humid chamber. The results suggest that relative humidity does not change only the length of the phosphate chains but also their affinity towards the available cations. At low relative humidity, zinc pyrophosphate to polyphosphate chains were formed compared to predominantly shorter iron orthophosphate chains at high relative humidity. In addition, relative humidity altered the structure of the mature tribofilm. At low relative humidity, the tribofilm had a patchy structure with average thickness of 140 nm and fractal dimension of 2.17. However, at high relative humidity, the tribofilm had a thin dendritic structure with average thickness of 85 nm and fractal dimension of 2.34. This means that the structure is more complex with a larger number of nesting self-similar structures at all scales. This is significant in making the transition from descriptive towards quantitative information of the tribofilm structure.

Keywords ZDDP antiwear · Tribofilm · Decomposition reactions · Raman · Water contamination

1 Introduction

Water, which can be present in the lubricating oil of any machinery, can have adverse effect on the overall efficiency of the lubricant and lubricated parts such as bearings in different ways [1]. For instance, water can increase wear and shorten the life of the lubricated parts [2], due to hydrogen embrittlement and oxidation. The extent of this damage depends on whether water is dissolved [3] or free [4].

There are numerous studies, which investigated the effect of relative humidity on real-life engines. For example, Chang et al. [5] showed that a 50% increase in relative humidity from ambient at 30% to a mild at 60% had a significant impact on the engine manifested mainly in retarding the combustion phasing along with reducing the NOx concentration. Similarly, Pekula et al. [6] showed that a threefold increase in the relative humidity can cause a reduction of NOx concentration by 15 to 20%.

✉ Abdel Dorgham
a.dorgham@leeds.ac.uk

[1] School of Mechanical Engineering, Institute of Functional Surfaces, University of Leeds, Leeds LS2 9JT, UK

Few previous studies have assessed the effect of relative humidity [3] and added free water [4, 7–9] on the performance of oil additives including zinc dialkyldithiophosphate (ZDDP). ZDDP is a highly efficient antiwear additive due to its formation of a thin (<150 nm) protective tribofilm on lubricated surfaces rubbing against each other [10–16]. Dorgham et al. [7] assessed the role of free water added to the lubricating oil in the reaction kinetics of ZDDP and how it can alter the resulting tribofilm. Water was found to initially increase the reaction kinetics of the ZDDP additive, but it had a permanent damaging effect on the formed zinc phosphate chains. Water can hinder the polymerisation of the hastily formed phosphate chains, which results in the formation of impotent short zinc orthophosphate chains unable to polymerise even if water evaporates from the oil. The authors related this to the weak bonds formed between the water molecules and the formed short phosphate chains because of the high affinity of water to dissolve in the phosphates [17]. Similarly, several previous studies [4, 8, 9], showed that the formed tribofilm in an oil containing free water consists of short zinc phosphate chains compared to longer ones when water is absent. The tribofilm was also found to be thinner in the presence of water [4]. Such a

detrimental effect was suggested to be a result of the competition of water with ZDDP molecules over the available steel surface, which delays the adsorption and decomposition of the ZDDP molecules on the steel substrate. This can significantly delay the formation and alter the physicochemical properties of the generated tribofilm. Fuller et al. [18] suggested that one of the adverse effects of water is its reaction with the initially formed long phosphate chains, which results in the formation of short iron phosphate.

Other few studies [3] investigated the impact of relative humidity on the decomposition reactions of ZDDP and demonstrated that as the relative humidity increased, the formed tribofilm was thinner and less tenacious with predominantly shorter zinc phosphate chains.

All the previous studies regarding the presence of water, whether free or dissolved, in the oil confirm that water affects both the kinetics of the decomposition reaction of ZDDP [7] as well as the physicochemical properties of the formed protective tribofilm by impeding the polymerisation of the short phosphate chains into longer ones [4, 4, 7–9]. However, the previous studies did not show whether the formed tribofilm consists of mainly zinc, iron, or mixed zinc and iron phosphate. In addition, the previous studies did not fully assess whether water can alter the tribofilm physical structure, nor did they link this to its composition, e.g. whether the tribofilm of short or long zinc, iron or mixed zinc and iron phosphate is smooth, rough, patchy, dendritic, etc.

In the absence of water, the ZDDP tribofilm was reported to have a structure of small and big ridges and valleys aligned and elongated along the rubbing direction [19–21]. The big and thick ridges consist of phosphate with long chains, but the shallow troughs were reported to have short chains [22–26]. These results indicate that there is a link relating the physical appearance to the chemical properties of the generated ZDDP tribofilm. However, so far, no previous studies assessed the effect of water on these combined parameters, which is expected to be significant. One of the major challenges is the difficulty in measuring the different features of the formed tribofilms, e.g. ridges and troughs, quantitatively. Previous reports tended to describe these features qualitatively, e.g. how they are elongated in the direction of rubbing. Such a lack of previous quantitative studies is related to the difficulties in obtaining different tribofilms with different chemistries and identifying different features in the formed tribofilms. This study aims at investigating this correlation by examining how humidity can alter the physicochemical characteristics of the formed ZDDP tribofilm over time using Raman spectroscopy and structure and thickness using atomic force microscopy (AFM). This should help better understand the combined impact of water on the physicochemical properties of the ZDDP tribofilms.

2 Materials and Methods

2.1 Lubricants

Poly-α-olefin (PAO) oil ($\rho = 830$ kg cm, $\eta = 4$ cSt at 100 °C.) with ZDDP antiwear additive was used as the main lubricant. The ZDDP additive was used at a low concentration in the oil with a resulting mix containing 800 ppm of phosphorus.

2.2 Standard P- and S-Based Samples

In order to quantify the decomposition species and thus the composition of the formed ZDDP tribofilms, which apart from phosphorus contain also sulphur species, several sulphur and phosphorus standard samples were used, which are listed in Tables 1 and 2, respectively. The sulphur samples were purchased, whereas the phosphorus samples were synthesised in house following the method described in detail elsewhere [27]. The synthesised samples were solid, but the purchased ones were obtained in a powder form with a high purity (Table 1). Prior to the surface analysis, the powder samples were ground and pressed into plates of diameter 5 mm and variable heights above 3 mm.

2.3 Pin-on-Disc Tribometer

Figure 1 shows the tribometer utilised to perform the tribological experiments, which is a pin-on-disc rig capable of simulating pure sliding conditions. The relative humidity was maintained using a chamber, which controlled the flow of humid and dry air to achieve the required level of humidity. The humidity sensor, which measured the humidity level, was placed inside the chamber during the entire tribological experiment. The operating conditions during the tribological tests are listed in Table 3. A bearing steel ball with a diameter 6.35 mm (Rq < 13 nm) was used as a pin on a bearing steel disc of a 40 mm diameter (Rq < 110 nm).

The tribological tests were performed at 80 °C. This was chosen to be lower than 100 °C at which evaporation of water from the oil occurs at a much faster rate [7, 9]. The humidity sensor had an accuracy within ±3%, whereas the accuracy of the temperature controller was within ±1 °C. The sliding speed during the tests was 600 ± 20 mm/s. The load was maintained at 60 N. Under these conditions, the maximum contact pressure was 2.5 GPa and the λ ratio was 0.18 ($\lambda \ll 1$), which indicated that the lubrication regime was boundary.

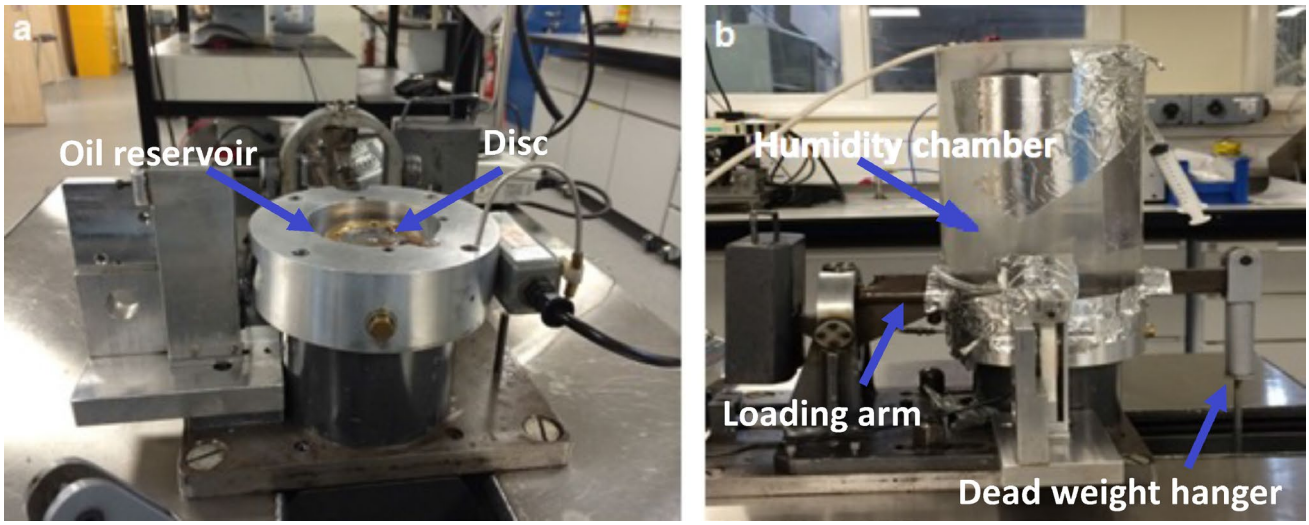

Fig. 1 Pin-on-disc rig **a** without and **b** with the humidity control system

Table 1 List of the different sulphur-based and metallic oxide samples used as standards for Raman spectroscopy

Material	Supplier	Purity
Zinc sulphide (ZnS)	Sigma-Aldrich	> 99.9%
Iron(II) sulphide (FeS)	Alfa Aesar	> 99.9%
Iron disulphide (FeS_2)	Sigma-Aldrich	> 99.8%
Pyrite (FeS_2)	Alfa Aesar	Natural[a]
Sphalerite ((Zn,Fe)S)	Alfa Aesar	Natural[a]
Zinc sulphate monohydrate $ZnSO_4 \cdot H_2O$	Sigma-Aldrich	> 99.9%
Iron (II) sulphate hydrate ($FeSO_4 \cdot xH_2O$)	Sigma-Aldrich	> 99.9%
Iron(III) sulphate hydrate $(Fe_2SO_4)_3 \cdot xH_2O$	Sigma-Aldrich	> 99.9%
Zinc oxide (ZnO)	Sigma-Aldrich	> 99.9%
Iron(III) oxide (Fe_2O_3)	Sigma-Aldrich	> 99.0%

[a]Purity could not be verified

2.4 Raman Spectroscopy

Raman spectroscopy (Renishaw InVia microscope) was performed using an excitation laser of 488 nm wavelength. The laser spot had a high spatial resolution < 1 µm. The acquisition was in the 100–1500 cm^{-1} Raman shift in which the antiwear films showed relevant (oxide, sulphide and phosphate) peaks. The acquisition time was fixed at 400 s using 5 and 10% laser power. The low laser power was chosen to avoid any sample degradation. The temperature of the measurements was controlled at 25 °C and the relative humidity was about 30% in an uncontrolled humid atmosphere. Before performing the experiments, a quick calibration using a Si(100) sample was performed in order to confirm that the Si peak is located at 520 cm^{-1}. Different types of spectra were acquired, which included single scans of points of

Table 2 List of the different synthesised phosphorus-based samples used as standards for Raman spectroscopy

Glass	Composition	O/P	M/P[a]	Chain length	Type
Zn metaphosphate	$0.5(ZnO) \cdot 0.5(P_2O_5$	3.0	0.50	∞	Amorphous
Zn polyphosphate	$0.57(ZnO) \cdot 0.43(P_2O_5)$	3.16	0.66	56	Amorphous
Zn pyrophosphate	$0.67(ZnO) \cdot 0.33(P_2O_5)$	3.52	1.02	3	Amorphous & crystalline
Zn orthophosphate	$0.75(ZnO) \cdot 0.25(P_2O_5)$	4.0	1.5	1	Crystalline
Fe $poly_{0.33}$-phosphate	$0.25(Fe_2O_3) \cdot 0.75(P_2O_5)$	3.0	0.33	∞	Crystalline
Fe $poly_{0.50}$-phosphate	$0.33(Fe_2O_3) \cdot 0.67(P_2O_5)$	3.24	0.49	5	Crystalline & Amorphous
Fe $poly_{0.67}$-phosphate	$0.40(Fe_2O_3) \cdot 0.60(P_2O_5)$	3.50	0.67	3	Amorphous
Fe $poly_{1.0}$-phosphate	$0.5(Fe_2O_3) \cdot 0.5(P_2O_5)$	4.0	1.0	1	Crystalline
Zn_{75} Fe_{25}-phosphate	$0.15(ZnO) \cdot 0.23(Fe_2O_3).0.62(P_2O_5)$	3.18	0.49	10	Amorphous
Zn_{50} Fe_{50}-phosphate	0.20(ZnO).0.14(Fe2O3).0.57(P2O5)	3.04	0.42	13	Amorphous
Zn_{25} Fe_{75}-phosphate	0.40(ZnO).0.07(Fe2O3).0.53(P2O5)	3.08	0.51	19	Amorphous

[a] Ratio between the atomic concentration of iron and zinc to the one of phosphorus

Table 3 Summary of the operating conditions for the tribological tests using the pin-on-disc tribometer

Operational variable	Value
Ball/disc material	AISI 52100
Ball diameter (mm)	6.35
Disc diameter (mm)	40
Ball roughness R_q (nm)	13
Disc roughness R_q (nm)	112
Lubricant	PAO + ZDDP
Temperature (°C)	80
Load (N)	60
Entrainment speed (mm/s)	600
Water (%RH)	30, 90
Time (minutes)	120

interest and maps. One of these regions was across the wear scar to check the heterogeneity of the tribofilm composition.

After acquiring the Raman spectra, a baseline subtraction was performed using a smooth spline that kept all the data points above zero. The spectra were then fitted with different Gaussian/Lorentzian peaks using WiRE 3.4 software (Renishaw, USA). The peaks were then assigned based on the standard samples listed in Tables 1 and 2 and the available literature [27, 28].

2.5 AFM

The structure of the formed tribofilms was examined at the microscale by a commercial AFM (Bruker Dimension Icon). The Antimony (n)-doped Si AFM cantilever was rectangular in shape with dimensions $125 \times 40 \times 5\ \mu m^3$. The cantilever had a spring constant of 28 ± 5 N/m. The cantilever tip, which was made of the same material of the cantilever, was a three-sided pyramid with a height of 15 µm and a nominal radius of 8 nm. The AFM images were acquired at 1 Hz speed scanning an area of $10 \times 10\ \mu m^2$ under a contact force less than 100 nN.

Using at least four AFM images of four scanned areas in the same sample, the fractal dimension of the formed tribofilms was calculated in order to compare the complexity of their structures and how they change with the scale using the following two methods:

- Cube counting In the cube counting method, the height of the tribofilm was scaled such that the distance between the minimum and maximum height, Z, in the scaled image equalled the x or y range, X and Y, respectively. Then, the 3D scaled surface was covered by cubic lattice with a lattice constant ϵ [29]. For instance, in the case of ϵ is set at $\ell/3$, where ℓ is the width or height of the cube, this results in a lattice of $3 \times 3 \times 3 = 27$ cubes. The total number of the cubes N, which were the ones that should necessarily contain one or more pixel of the image, were used to find the surface area $A = N\epsilon^2$. The lattice constant ϵ was selected to be infinitely small. However, as the smallest component of any image is the pixel, ϵ was reduced systematically by factors of 2 until reaching the length of two adjacent pixels. In this case, the fractal dimension D_f was calculated as follows [30]:

$$D_f = \lim_{\epsilon \to 0} \frac{\log N(\epsilon)}{\log (1/\epsilon)} \tag{1}$$

- Triangulation instead of cubes as in the cube counting method, triangles of unit dimension ϵ were used. The total number of the triangles N was used to find the surface area $A(\epsilon)$. Then, the fractal dimension D_f was calculated as follows [30]:

$$D_f = \lim_{\epsilon \to 0} \frac{\log A(\epsilon)}{\log (1/\epsilon)} + 2 \tag{2}$$

The AFM analysis was performed using Gwyddion v2.55 software.

3 Results

3.1 Effect of Water on Tribofilm Structure

The generated tribofilms using the pin-on-disc rig at 80 °C were analysed using the AFM. Figure 2 shows the AFM topography maps of the ZDDP tribofilms generated after 1, 5 and 80 min of rubbing under two relative humidities of 30 and 90%. During short rubbing times, i.e. after 1 and 5 minutes, the tribofilm does not have a patchy structure, but appears thin and uniform regardless of the humidity level. However, after long rubbing time, i.e. after 80 min, the tribofilm appears patchy with ridges of different sizes protruding from the tribofilm. The evolution of the tribofilm structure from continuous to patchy was reported before [31]. Apart from this general trend, there were noticeable differences between the structures of the mature tribofilms formed after 80 min of rubbing at 30 and 90% of relative humidity. The tribofilm formed at low relative humidity shows the typical patchy structure, which is significantly different from the dendritic structure formed at high relative humidity. One way to quantify the difference between these patchy and dendritic-like structures is by calculating their fractal dimensions, which measure the complexity of nesting self-similar structures at different scales. Two methods, i.e. cube counting [29, 32] and triangulation [29], were utilised to estimate the fractal dimensions, which are presented in Table 4. The tribofilm formed at relative humidity of 30% was estimated

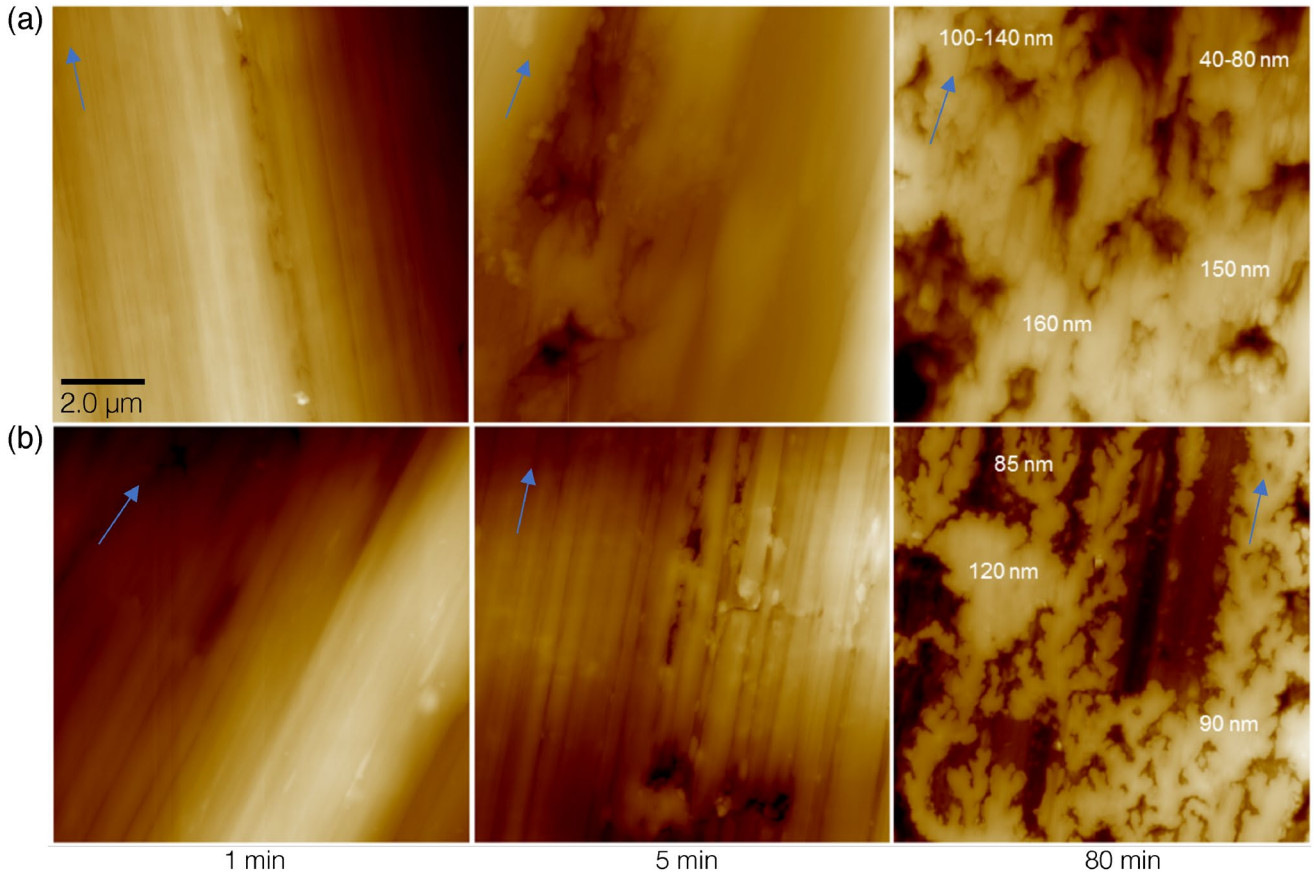

Fig. 2 AFM topography maps (10×10 µm^2) of the evolution of the tribofilm over time at different levels of relative humidity of **a** 30% (top panel) and **b** 90% (bottom panel). Arrows indicate the direction of sliding

to have a fractal dimension of 2.17. This was about 7.83% smaller than that formed at 90% relative humidity, which was estimated to have a fractal dimension of 2.34. This increased fractal dimension when water is present suggesting that the tribofilm has a more complex structure with a larger number of nesting self-similar features at all scales. The fractal dimension appears to bear information about the formation history of the tribofilm, which suggests that a link between the fractal dimension and other mechanical properties of the tribofilm, e.g. elastic modulus and hardness, might be possible. Therefore, the fractal dimension results are important not only as a tool to compare the different structures in terms of complexity and shape, but also as a means to bring about the transition from the descriptive information of the tribofilm structure to the quantitative information.

The thickness at different locations across the formed tribofilms is shown in Fig. 3. The results show that the high relative humidity reduced the tribofilm thickness notably. The average tribofilm thickness at relative humidity of 90% was 85 nm, whereas at 30% the thickness was about 140 nm. It should be noted that these values represent the height difference between the ridges and troughs. As suggested by Bec et al. [20], troughs can have an average thickness of 30 nm, which can be added to the thickness values shown in Fig. 3. The reduction in the tribofilm thickness due to the mixed water with oil matches the findings of numerous studies indicating a limiting effect of water hindering the growth of ZDDP tribofilms [3, 4, 8, 9]. This was related to the competition between water and ZDDP molecules over the steel surface. The polar water molecules reaches the surface first, which delays the adsorption and decomposition of the additive molecules at the substrate, and subsequently delays the formation of the protective tribofilm. Alternatively, other studies [7] suggested that water can suppress the chemical reactivity of the initially formed PO_2^- groups, which can inhibit the formation of the phosphate layers.

3.2 Surface Analysis

3.2.1 Standard Samples

The Raman spectra of several sulphur-based samples, which of similar composition to the decomposition species that are expected to be found in the ZDDP tribofilm, are shown

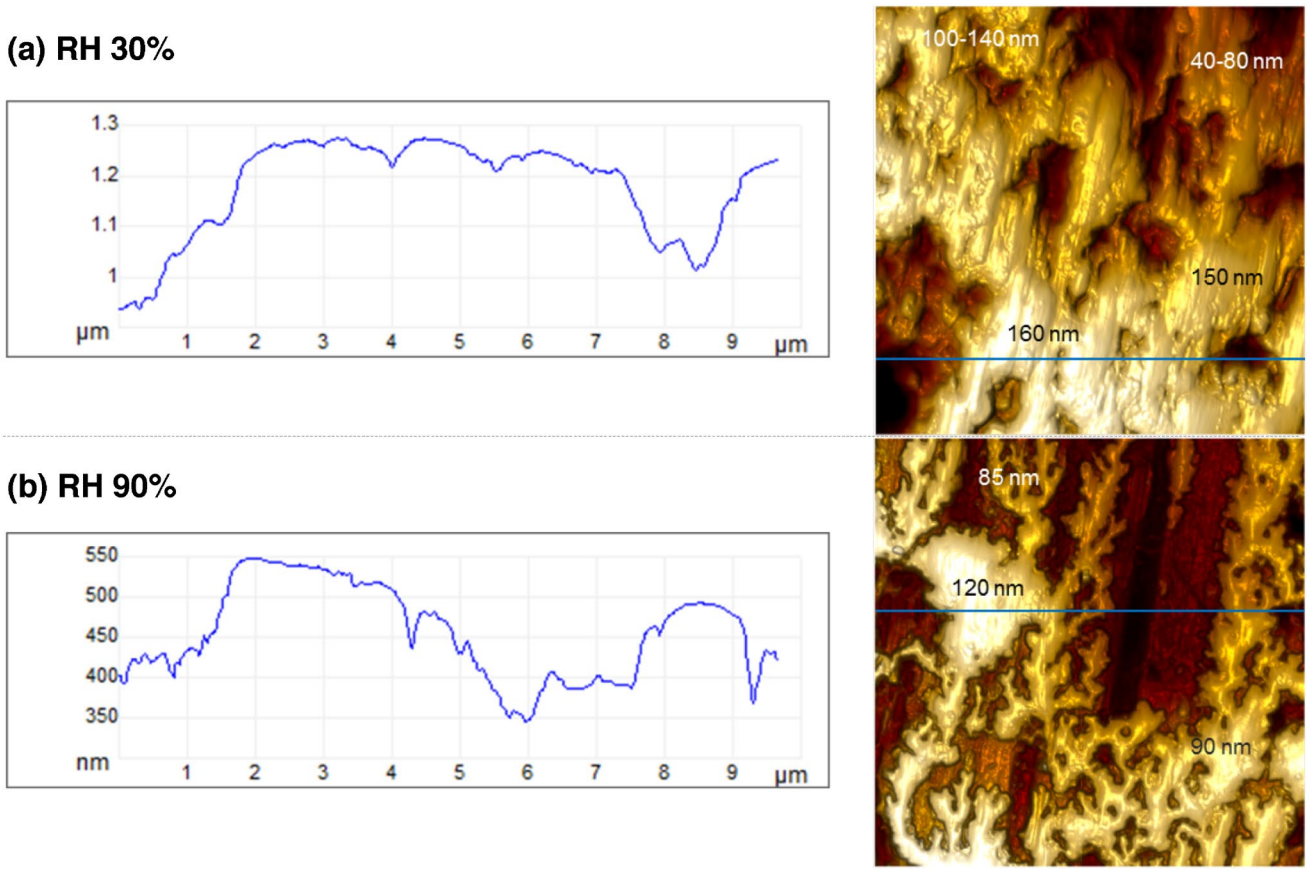

Fig. 3 AFM topography maps and profiles of the mature tribofilm, i.e. after 80 minutes of rubbing time, at different levels of relative humidity; 30% top and 90% bottom

Table 4 Fractal analysis of the mature tribofilm, i.e. after 80 min of rubbing time, at two different levels of relative humidity, i.e. 30% and 90%

Method	Dimension		Difference (%)
	30% RH	90% RH	
Cube counting [29, 32]	2.14	2.30	7.48
Triangulation [29]	2.20	2.37	7.73
Average	2.17	2.34	7.83

in Fig. 4. Generally, the spectra show that the main peaks across the different samples appear below 500 cm^{-1}. These peaks might be related to iron/zinc oxide, sulphide or sulphate depending on the number of peaks and their Raman shifts.

The Raman spectra of the standard phosphorus-based samples of zinc, iron and mixed zinc and iron phosphate are presented in Fig. 5. A summary of the positions and assignments of the main phosphate peaks is listed in Table 5. Generally, the peaks appear sharp having small full width at half maximum (FWHM) in the case of crystalline samples, whereas they appear wide with large FWHM in the case of amorphous samples. The spectra show six main peaks, as follows:

- The first peak appears as a single or multiple peaks below 400 cm^{-1}. This matches the ($\delta PO_4^{3}-$) bending mode of the phosphate matrix.
- The second peak appears around 710–760 cm^{-1}. This matches the symmetric stretching mode ($\nu_s PO_3^{2-}$) of Q^1 units. The structural units Q^n are good indicators of the average chain length n. In the case of no branching, every chain consists of two end groups Q^1 and $n-2$ middle groups Q^2, and possibly some isolated Q^0 units.
- The third peak appears around 960–1010 cm^{-1}. The peak location matches the P=O asymmetric stretching mode ($\nu_{as} PO_4^{3-}$) of Q^0 units.
- Two other peaks appear in the range 1010–1150 cm^{-1} and 1150-1210 cm^{-1}. The positions of these peaks match the ($\nu_s PO_3^{2-}$) symmetric and ($\nu_{as} PO_3^{2-}$) asymmetric stretching modes of Q^1 units of P-O-P, respectively. The latter peak around 1150–1210 cm^{-1} may equally be assigned to the ($\nu_s PO_2^{-}$) symmetric stretching mode.

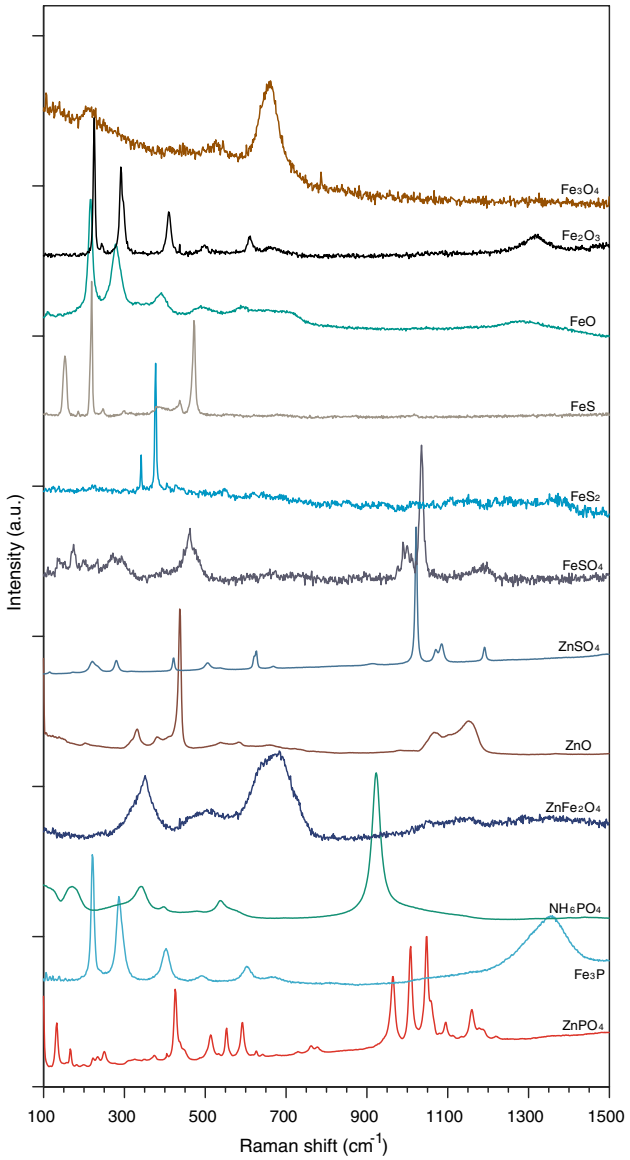

Fig. 4 Raman spectra of the different sulphur-based and metallic oxide samples used as standards for Raman spectroscopy

Table 5 Raman shifts assignments of the zinc, iron and mixed zinc and iron phosphate glasses

Raman shift (cm^{-1})	Assignment	Q	Ref.
360	δPO_4^3-	–	[33–35]
710	$\nu_s PO_3^{2-}$	Q^1	[34]
970	$\nu_{as} PO_4^3-$	Q^0	[28, 34, 36]
1140	$\nu_s PO_3^{2-}$	Q^1	[35, 37]
1190	$\nu_{as} PO_3^{2-}$, $\nu_s PO_2^-$	Q^1	[37]
1280	$\nu_{as} PO_2^-$	Q^2	[35, 37]

- Another peak appears in the high Raman shift area around 1260–1300 cm^{-1} linked to the ($\nu_{as} PO_2^-$) asymmetric stretching mode of Q^2 units.

Figure 6 follows the change in the Raman shifts of the two main peaks of $\nu_s PO_3^{2-}$ at 710 cm^{-1} and $\nu_s PO_2^-$ at 1200 cm^{-1} of the various phosphate glasses with different chain lengths and different metallic cations (zinc, iron or mixed zinc and iron). The Raman shifts of the $\nu_s PO_3^{2-}$ and $\nu_s PO_2^-$ peaks of the long zinc phosphate chains start at 710 and 1202 cm^{-1}, respectively. As the chain length becomes shorter and as iron replaces zinc, the Raman shift of $\nu_s PO_3^{2-}$ increases, whereas one of $\nu_s PO_2^-$ decreases, both linearly, until reaching 814 and 1010 cm^{-1} in the case of short chain iron $poly_{100}$phosphate.

These results indicate that the position of the Raman peaks of $\nu_s PO_3^{2-}$ at 710 cm^{-1} and $\nu_s PO_2^-$ at 1200 cm^{-1} has the potential to be used as a quantification tool for the phosphate chain length, i.e. the longer the length of the chains the lower the Raman shift of $\nu_s PO_3^{2-}$ and the higher the Raman shift of $\nu_s PO_2^-$. Similarly, Smith et al. [38, 39] showed that the larger the chain length the higher the Raman shift of the $\nu_s PO_2^-$ stretch peak frequency. The increase in Raman shift frequency was associated with the overall decrease in the terminal/external P-NBO (non-bridging oxygen) bond length because generally the short bonds tend to vibrate at higher frequency than the longer bonds [40]. Another reason for the change in frequency might be due to the change in the cationic potential of the phosphate metal oxide (metal cations), which as it increases, the phosphorus shielding decreases due to the depletion the electron density on phosphorus [39].

The results shown in Fig. 6 indicate that as iron replaces zinc, the phosphate chain length decreases significantly. Similarly, numerous previous studies [38, 39, 41, 42] showed that the presence of metallic cations, e.g. FeO or ZnO, in phosphate glasses reduces the phosphate chains length. In the case of zinc phosphate, as an example, zinc shares the oxygen of the phosphate, as follows [39]:

$$P{-}O{-}P + Zn{-}O \rightarrow P{-}O{-}Zn{-}O{-}P \quad (3)$$

This highlights the role of metallic cations in the depolymerisation of long chains of zinc or zinc/iron phosphate.

3.2.2 ZDDP Tribofilm

The Raman spectra of the mature tribofilms formed at relative humidity of 30 and 90% are presented in Fig. 7a and b, respectively. The peaks that appear at small Raman shifts between 100 and 400 cm^{-1} can be ascribed to the network bending of the glass [33–35] or to iron and zinc oxide, sulphide and sulphate as shown in Fig. 4 using the standard samples. The peaks appearing around 420, 566 and 634 cm^{-1} correspond to bending vibrations of PO_4 network,

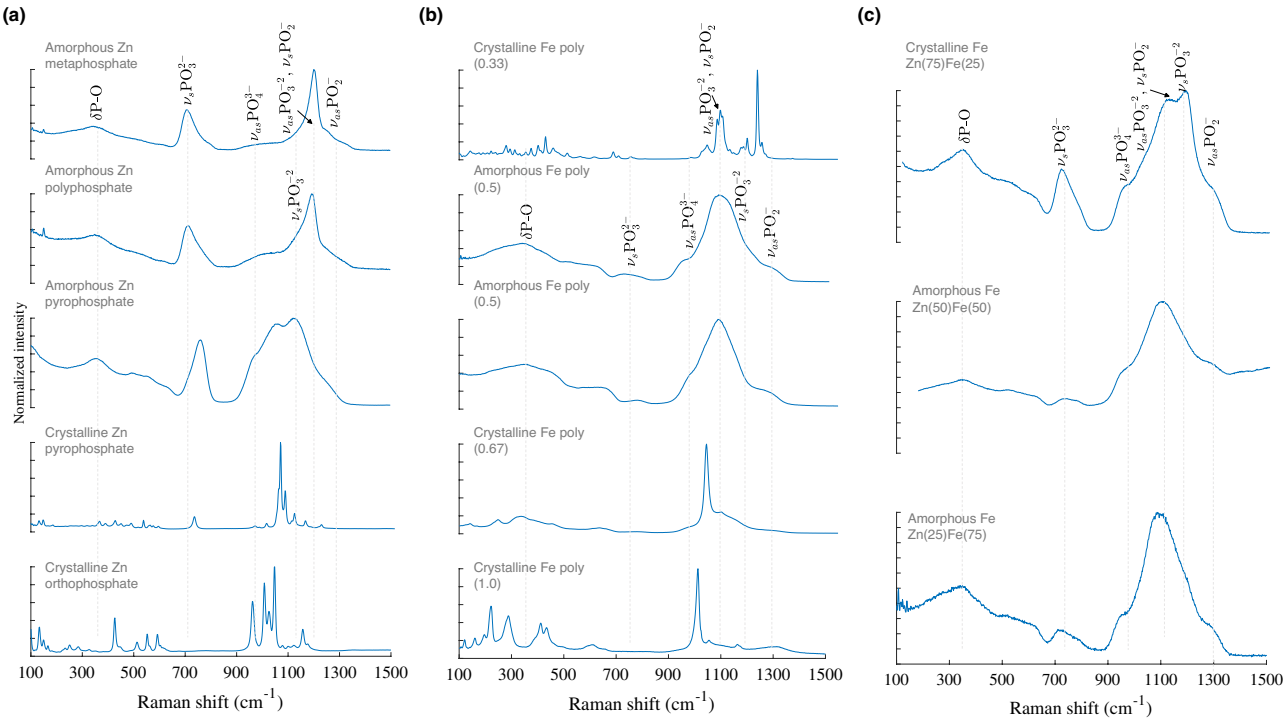

Fig. 5 Raman spectra of the different zinc, iron and mixed zinc and iron phosphate glasses used as standards for Raman spectroscopy

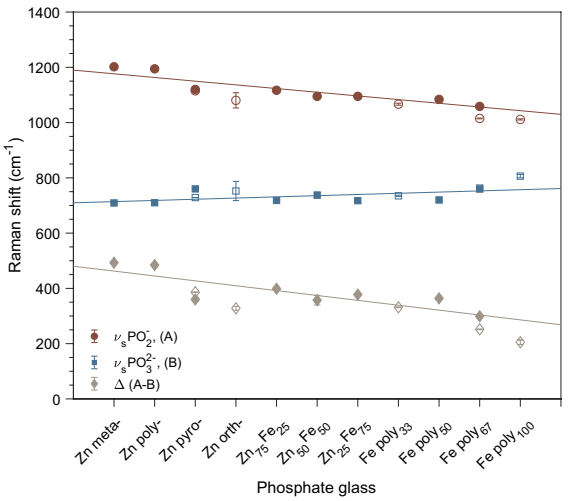

Fig. 6 Raman shift evolution of the two main peaks: $\nu_s PO_3^{2-}$ at 710 cm^{-1} and $\nu_s PO_2^-$ at 1200 cm^{-1}, and their Raman shifts difference, across the amorphous (closed symbols) and crystalline (open symbols) phosphate glasses

as reported before [33–35] and also shown in Fig. 6 using the synthesised metallic phosphates. These peaks can also be assigned equally to different modes of bending within $(O-P-O)_{asm}$, $(O\text{-}P\text{-}O)_{sym}$ and $(P-O-P)_{sym}$ [37]. The other peaks around 710, 970, 1140, 1190 and 1280 cm^{-1} were ascribed to different modes of stretching within the phosphate chains, as listed in Table 5.

Several general observations can be noted from the maps of Raman spectra across the mature ZDDP tribofilms formed after 80 minutes of rubbing at 30 and 90% relative humidity as shown in Fig. 7c and d, respectively. First, at relative humidity of 90%, Raman shifts below 600 cm^{-1} as well as those between 1100 cm^{-1} and 1400 cm^{-1} do not appear uniform compared to the ones at lower relative humidity. The reason behind this is not fully understood. Another interesting observation is that at high relative humidity, the Raman shifts at 650 and 950 cm^{-1} appear sharper, i.e. having small FWHM, and more uniform in width and height compared to those at low relative humidity. The sharp peak at 950 cm^{-1} at high relative humidity corresponds to P=O asymmetric stretching mode ($\nu_{as}PO_4^3-$) of Q^0 units. No overlapping peaks at higher Raman shifts were observed, which indicates the absence of Q^1 and Q^2 units corresponding to long phosphate chains. This suggests that the majority of the tribofilm formed at high relative humidity consists of short orthophosphate with iron as metallic cation. This assignment of iron instead of zinc phosphate is based on the peak position, which was found to be shifted to a value lower than 950 cm^{-1} at high humidity, whereas it shifted to higher values at low humidity. In addition, the Raman spectra at high humidity have distinctive sharp peaks, which are similar to the previously reported spectra for iron phosphate [34].

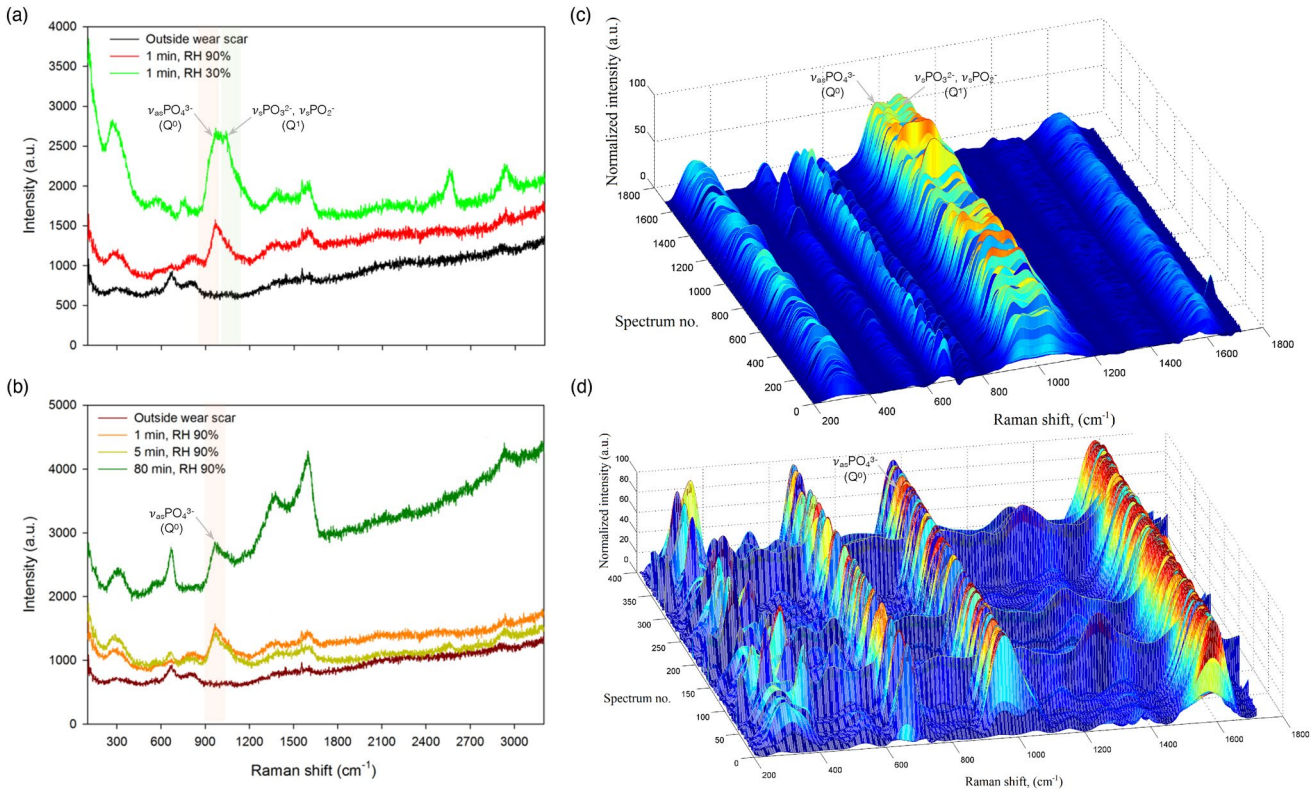

Fig. 7 Raman spectra at different spots of the ZDDP tribofilm: **a** after 1 minutes of rubbing at 30 and 90% relative humidity, **b** after 1, 5 and 80 min of rubbing at 90% relative humidity, **c** and **d** spectra at different location acquired after 80 minutes of rubbing time at relative humidity of 30 and 90%, respectively

In the case of low relative humidity, the shape of the spectra around 950 cm^{-1} shows the presence of multiple overlapping peaks extends beyond 1100 $^{-1}$. This was also reported in several previous studies [28, 34, 36], which assigned the peak to amorphous zinc phosphate. The wide overlapping $\nu_s PO_2^-$ and $\nu_{as}PO_{4^{3-}}$ phosphate peaks at low Raman shifts indicates that most of the tribofilm consists mainly of zinc pyro- to polyphosphate, with possibly a small amount of iron phosphate.

4 Discussion

The mechanism of how relative humidity can affect the reaction kinetics of ZDDP and the composition of its formed tribofilm is summarised in Fig. 8. Initially, as rubbing started a relatively thick oxide layer, which is about 7 nm in thickness exists on the steel surface [14]. This layer will be in direct contact with the PAO lubricating oil, which contains ZDDP molecules in addition to dissolved and free water due to the relative humidity.

The ZDDP molecules is considered to consist of a polar moiety and a non-polar alkyl tail [43]. This causes the ZDDP molecule to have high polarity. Therefore, both ZDDP and water molecules will have a high affinity to steel surfaces. However, as water molecules have larger polarity, they will have larger affinity to the steel substrate than ZDDP. Therefore, at high relative humidity, the largely available water in the oil competes with ZDDP and delays its adsorption to the steel surface because water adsorbs and covers the surface faster than the additive. Subsequently, water delays the formation of the protective tribofilm until more water evaporates from the oil with time as rubbing continues. Over time, more free sites on the steel surface become available for the additive adsorption and its subsequent decomposition on the surface to form initially zinc/iron sulphate and sulphate species and then short chain iron orthophosphate. As more water evaporates, the short chains do not polymerise into longer ones [3, 4, 7–9] due to the formation of weak bonds between the newly formed short phosphate chains and water molecules [7]. Water does not evaporate completely due to its high affinity to dissolve in the phosphates [17].

On the other hand, at low relative humidity, ZDDP can adsorb to the steel surface without delay. The molecules then decompose to form iron/zinc sulphate, which then reduces into sulphides [44, 45], before ultimately form short chains zinc orthophosphate. As rubbing continues, the short chains polymerise to form longer zinc pyrophosphate chains, which

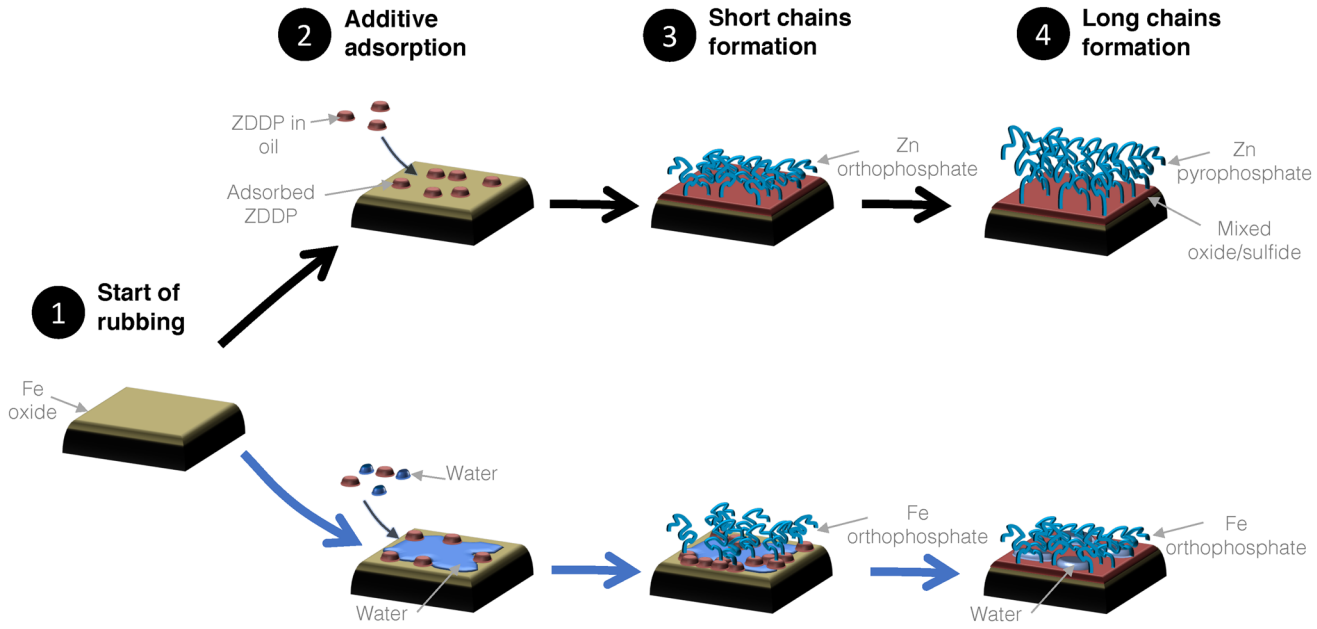

Fig. 8 Schematic summarising of the effect of relative humidity on the different stages of the decomposition reaction of ZDDP and its formed protective antiwear tribofilm

over rubbing can further polymerise into longer polyphosphate chains [14].

The dendritic-like structure formed at high relative humidity compared to the patchy one at low relative humidity can be mainly related to the change in the oil polarity mainly because of the relatively high water content in the oil at high relative humidity. Several previous studies [46, 47] examined the influence of oil polarity on different aspects of ZDDP including its adsorption and reactions, which showed that the tribofilm formation is accelerated in oils with low polarity. The resulting tribofilms were found to be of larger thickness and roughness compared to those in polar oils [48]. They related such effect to the absence of competition that can occur between the ZDDP molecules and the non-polar oil on the steel surface thus allowing the ZDDP molecules to adsorb faster and more efficiently. The effect of oil polarity was found to also exhibit a substantial influence on the chemical characteristics of the formed tribofilms. Although, the tribofilms that are formed in either polar or non-polar oils were found to consist primarily of phosphate, still significant differences were found in the resulting sulphur in the tribofilm. In polar oils, mainly sulphide is generated, whereas in non-polar oils both sulphide and sulphate can form [43].

All the aforementioned studies confirm that any change in the oil polarity, which can be achieved by changing the oil type or adding high concentration of water or high relative humidity, can have considerable effects on the structure of the generated tribofilm. Furthermore, the dendritic-like structure formed at high relative humidity compared to the patchy one at low relative humidity suggests that the initially adsorbed water molecules on the steel surface do not completely evaporate at the subsequent stages of the tribological test due to its has high affinity to dissolve in the phosphates [17]. This prevents the additive decomposition on big parts of the steel surface, which ultimately results in less surface coverage of the formed tribofilm and its final dendritic-like structure.

5 Conclusion

This study examined the impact of relative humidity on the physical structure and chemical characteristics of ZDDP antiwear films. At low relative humidity, the tribofilm had a patchy structure of a fractal dimension of 2.17 and average thickness of 140 nm. However, at high relative humidity, the tribofilm had a thin dendritic structure of a fractal dimension of 2.34 and average thickness of 85 nm. This means that the formed structure at high relative humidity is more complex with larger number of nesting self-similar structures at all scales. These findings are important in making the transition between the descriptive information of the tribofilm structure and the quantitative one. Furthermore, the Raman spectroscopy results suggested that at small relative humidity most of the tribofilm consisted mainly of zinc phosphate compared to iron phosphate at high level of relative humidity. This suggests that relative humidity predetermines the nature, type and chain length of the formed phosphate species within the tribofilm.

Supplementary Information The online version contains supplementary material available at (https://doi.org/10.1007/s11249-021-01446-6).

References

1. Duncanson, M.: Detecting and controlling water in oil. In: Proceedings of Noria Lubrication Excellence 2005 Conference April 25–29. San Antonio, Texas (2005)
2. Sheehan, P.: The wear kinetics of NaCl under dry nitrogen and at low humidities. Chem. Phys. Lett. **410**, 151–155 (2005)
3. Parsaeian, P., Van Eijk, M.C., Nedelcu, I., Neville, A., Morina, A.: Study of the interfacial mechanism of ZDDP tribofilm in humid environment and its effect on tribochemical wear. Part I: experimental. Tribol. Int. **107**, 135–143 (2017)
4. Parsaeian, P., et al.: An experimental and analytical study of the effect of water and its tribochemistry on the tribocorrosive wear of boundary lubricated systems with ZDDP-containing oil. Wear **358**, 23–31 (2016)
5. Chang, Y., Mendrea, B., Sterniak, J., Bohac, S.V.: Effect of ambient temperature and humidity on combustion and emissions of a spark-assisted compression ignition engine. J. Eng. Gas Turbines Power **139**, 051501 (2017)
6. Pekula, N., Kuritz, B., Hearne, J., Marchese, A., Hesketh, R.: The effect of ambient temperature, humidity, and engine speed on idling emissions from heavy-duty diesel trucks. SAE transactions, pp. 148–158 (2003)
7. Dorgham, A. et al.: On the decomposition reactions of ZDDP tribofilms—Part A: effect of added water. Tribol. Int. (2020)
8. Nedelcu, I., Piras, E., Rossi, A., Pasaribu, H.: XPS analysis on the influence of water on the evolution of zinc dialkyldithiophosphate-derived reaction layer in lubricated rolling contacts. Surf. Interface Anal. **44**, 1219–1224 (2012)
9. Cen, H., Morina, A., Neville, A., Pasaribu, R., Nedelcu, I.: Effect of water on ZDDP anti-wear performance and related tribochemistry in lubricated steel/steel pure sliding contacts. Tribol. Int. **56**, 47–57 (2012)
10. Dorgham, A., Neville, A., Morina, A.: In: Advanced Analytical Methods in Tribology, pp. 159–214. Springer (2018)
11. Spikes, H.: The History and Mechanisms of ZDDP. Tribol. Lett. **17**, 469–489 (2004)
12. Barnes, A.M., Bartle, K.D., Thibon, V.R.: A review of zinc dialkyldithiophosphates (ZDDPS): characterisation and role in the lubricating oil. Tribol. Int. **34**, 389–395 (2001)
13. Dorgham, A., et al.: Single-asperity study of the reaction kinetics of P-based triboreactive films. Tribol. Int. **133**, 288–296 (2019)
14. Dorgham, A., Azam, A., Morina, A., Neville, A.: On the transient decomposition and reaction kinetics of zinc dialkyldithiophosphate. ACS Appl. Mater. Interfaces **10**, 44803–44814 (2018)
15. Dorgham, A., Wang, C., Morina, A., Neville, A.: 3D tribo-nanoprinting using triboreactive materials. Nanotechnology **30**, 095302 (2019)
16. Dorgham, A.: Reaction kinetics and rheological characteristics of ultra-thin P-based triboreactive films PhD thesis (University of Leeds, 2018)
17. Bell, J., Delargy, K., Seeney, A.: Paper IX (ii) The removal of substrate material through thick zinc dithiophosphate anti-wear films. Tribol. Seri. **21**, 387–396 (1992)
18. Fuller, M.L.S., Kasrai, M., Bancroft, G.M., Fyfe, K., Tan, K.H.: Solution decomposition of zinc dialkyl dithiophosphate and its effect on antiwear and thermal film formation studied by X-ray absorption spectroscopy. Tribol. Int. **31**, 627–644 (1998)
19. Warren, O., Graham, J., Norton, P., Houston, J., Michalske, T.: Nanomechanical properties of films derived from zinc dialkyldithiophosphate. Tribol. Lett. **4**, 189–198 (1998)
20. Bec, S., et al.: Relationship between mechanical properties and structures of zinc dithiophosphate anti-wear films. Proc. R. Soc. Lond. A **455**, 4181–4203 (1999)
21. Graham, J., McCague, C., Norton, P.: Topography and nanomechanical properties of tribochemical films derived from zinc dialkyl and diaryl dithiophosphates. Tribol. Lett. **6**, 149–157 (1999)
22. Canning, G., et al.: Spectromicroscopy of tribological films from engine oil additives. Part I. Films from ZDDP's. Tribol. Lett. **6**, 159–169 (1999)
23. Nicholls, M.A., et al.: Chemomechanical properties of antiwear films using X-ray absorption microscopy and nanoindentation techniques. Tribol. Lett. **17**, 245–259 (2004)
24. Nicholls, M., et al.: Nanometer scale chemomechanical characterization of antiwear films. Tribol. Lett. **17**, 205–216 (2004)
25. Nicholls, M.A., Do, T., Norton, P.R., Kasrai, M., Bancroft, G.: Review of the lubrication of metallic surfaces by zinc dialkyldithiophosphates. Tribol. Int. **38**, 15–39 (2005)
26. Nicholls, M.A., et al.: Spatially resolved nanoscale chemical and mechanical characterization of ZDDP antiwear films on aluminum? Silicon alloys under cylinder/bore wear conditions. Tribol. Lett. **18**, 261–278 (2005)
27. Crobu, M., Rossi, A., Mangolini, F., Spencer, N.D.: Tribochemistry of bulk zinc metaphosphate glasses. Tribol. Lett. **39**, 121–134 (2010)
28. Berkani, S., et al.: Structural changes in tribo-stressed zinc polyphosphates. Tribol. Lett. **51**, 489–498 (2013)
29. Douketis, C., Wang, Z., Haslett, T.L., Moskovits, M.: Fractal character of cold-deposited silver films determined by low-temperature scanning tunneling microscopy. Phys. Rev. B **51**, 11022 (1995)
30. Theiler, J.: Estimating fractal dimension. JOSA A **7**, 1055–1073 (1990)
31. Zhang, Z., Yamaguchi, E., Kasrai, M., Bancroft, G.: Tribofilms generated from ZDDP and DDP on steel surfaces: Part 1, growth, wear and morphology. Tribol. Lett. **19**, 211–220 (2005)
32. Zahn, W., Zösch, A.: The dependence of fractal dimension on measuring conditions of scanning probe microscopy. Fresenius J. Anal. Chem. **365**, 168–172 (1999)
33. Shakhvorostov, D., et al.: On the pressure-induced loss of crystallinity in orthophosphates of zinc and calcium. J. Chem. Phys. **128**, 074706 (2008)
34. Zhang, L., Brow, R.K.: A raman study of ironphosphate crystalline compounds and glasses. J. Am. Ceram. Soc. **94**, 3123–3130 (2011)
35. Chakraborty, S., Arora, A.K.: Temperature evolution of Raman spectrum of iron phosphate glass. Vib. Spectrosc. **61**, 99–104 (2012)

36. Gauvin, M., et al.: Zinc phosphate chain length study under high hydrostatic pressure by Raman spectroscopy. J. Appl. Phys. **101**, 063505 (2007)
37. Lai, Y., Liang, X., Yang, S., Wang, J., Zhang, B.: Raman spectra study of iron phosphate glasses with sodium sulfate. J. Mol. Struct. **1013**, 134–137 (2012)
38. Smith, C.E., Brow, R.K.: The properties and structure of zinc magnesium phosphate glasses. J. Non-Cryst. Solids **390**, 51–58 (2014)
39. Smith, C.E., Brow, R.K., Montagne, L., Revel, B.: The structure and properties of zinc aluminophosphate glasses. J. Non-Cryst. Solids **386**, 105–114 (2014)
40. Popović, L., De Waal, D., Boeyens, J.: Correlation between Raman wavenumbers and P-O bond lengths in crystalline inorganic phosphates. J. Raman Spectrosc. **36**, 2–11 (2005)
41. Tsuchida, J., Schneider, J., Rinke, M.T., Eckert, H.: Structure of ternary aluminum metaphosphate glasses. J. Phys. Chem. C **115**, 21927–21941 (2011)
42. Khor, S., Talib, Z., Daud, W., Sidek, H.: Degradation study on ternary zinc magnesium phosphate glasses. J. Mater. Sci. **46**, 7895–7900 (2011)
43. Naveira-Suarez, A., et al.: The influence of base oil polarity and slide-roll ratio on additive-derived reaction layer formation. Proc. Inst. Mech. Eng. Part J 225:565–576, (2011)
44. Dorgham, A., Neville, A., Ignatyev, K., Mosselmans, F., Morina, A.: An in situ synchrotron XAS methodology for surface analysis under high temperature, pressure, and shear. Rev. Sci. Instrum. **88**, 015101 (2017)
45. Dorgham, A., et al.: In situ synchrotron XAS study of the decomposition kinetics of ZDDP triboreactive interfaces. RSC Adv. **8**, 34168–34181 (2018)
46. Tomala, A., Naveira-Suarez, A., Gebeshuber, I.C., Pasaribu, R.: Effect of base oil polarity on micro and nanofriction behaviour of base oil+ ZDDP solutions. Tribology **3**, 182–188 (2009)
47. Suarez, A.N., Grahn, M., Pasaribu, R., Larsson, R.: The influence of base oil polarity on the tribological performance of zinc dialkyl dithiophospate additives. Tribol. Int. **43**, 2268–2278 (2010)
48. Kar, P., Asthana, P., Liang, H.: Formation and characterization of tribofilms. J. Tribol. **130**, 042301 (2008)